The finding that *Prochlorococcus* releases DNA within membrane vesicles suggests that they may also serve as a reservoir of genetic information and possible vector for horizontal gene transfer in marine systems. To characterize the nature of the vesicle-associated DNA pool in natural seawater, we sequenced the "metagenome" from purified and DNase-treated vesicles isolated from our two field sites. Based on the unique sequences recovered, these "wild" vesicles contained a diverse pool of DNA with significant homology to members of 33 phyla from all three domains, although bacterial sequences were dominant (table S5). The majority of unique bacterial sequences were most similar to members of the *Proteobacteria*, *Cyanobacteria*, and *Bacteroidetes*. Since *Prochlorococcus* and other bacteria (*29*) export fragments of their genome within vesicles, the taxonomic diversity of DNA we observed in the field samples implies that diverse marine microbes release vesicles. We also identified sequences with homology to tailed and other marine phage, despite the fact that these were not apparent in the fractions by TEM (table S5 and supplementary text). Although we cannot completely rule out the presence of phage in the samples, these sequences could reflect either the export of prophage sequences within vesicles or DNA arising from phage infection of vesicles in the field.

Although membrane vesicles constitute only a fraction of the $>10^9$ small (<200-nm) colloidal particles per ml observed in seawater (*30*), that they are known to move diverse compounds between organisms in other systems (*5*, *7*) suggests that they could serve specific functions in marine ecosystems. By transporting relatively high local concentrations of compounds, providing binding sites, or acting as reactive surfaces, vesicles may mediate interactions between microorganisms and their biotic and abiotic environment that would otherwise be impossible in the extremely dilute milieu of the oligotrophic oceans.

References and Notes

1. B. L. Deatherage, B. T. Cookson, *Infect. Immun.* **80**, 1948–1957 (2012).
2. A. Kulp, M. J. Kuehn, *Annu. Rev. Microbiol.* **64**, 163–184 (2010).
3. J. W. Schertzer, M. Whiteley, *MBio* **3**, e00297-11 (2012).
4. I. A. MacDonald, M. J. Kuehn, *J. Bacteriol.* **195**, 2971–2981 (2013).
5. J. L. Kadurugamuwa, T. J. Beveridge, *J. Bacteriol.* **177**, 3998–4008 (1995).
6. J. Rivera *et al.*, *Proc. Natl. Acad. Sci. U.S.A.* **107**, 19002–19007 (2010).
7. L. M. Mashburn, M. Whiteley, *Nature* **437**, 422–425 (2005).
8. H. Yonezawa *et al.*, *BMC Microbiol.* **9**, 197 (2009).
9. Y. Gorby *et al.*, *Geobiology* **6**, 232–241 (2008).
10. A. J. Manning, M. J. Kuehn, *BMC Microbiol.* **11**, 258 (2011).
11. J. A. Roden, D. H. Wells, B. B. Chomel, R. W. Kasten, J. E. Koehler, *Infect. Immun.* **80**, 929–942 (2012).
12. G. L. Kolling, K. R. Matthews, *Appl. Environ. Microbiol.* **65**, 1843–1848 (1999).
13. C. Rumbo *et al.*, *Antimicrob. Agents Chemother.* **55**, 3084–3090 (2011).
14. P. Flombaum *et al.*, *Proc. Natl. Acad. Sci. U.S.A.* **110**, 9824–9829 (2013).
15. F. Partensky, L. Garczarek, *Annu. Rev. Mar. Sci.* **2**, 305–331 (2010).
16. Materials and methods are available as supplementary material on *Science* on the Web.
17. D. Mug-Opstelten, B. Witholt, *Biochim. Biophys. Acta* **508**, 287–295 (1978).
18. B. A. S. Van Mooy, G. Rocap, H. F. Fredricks, C. T. Evans, A. H. Devol, *Proc. Natl. Acad. Sci. U.S.A.* **103**, 8607–8612 (2006).
19. N. Borch, D. Kirchman, *Aquat. Microb. Ecol.* **16**, 265–272 (1999).
20. E. Tanoue, S. Nishiyama, M. Kamo, A. Tsugita, *Geochim. Cosmochim. Acta* **59**, 2643–2648 (1995).
21. H. X. Chiura, K. Kogure, S. Hagemann, A. Ellinger, B. Velimirov, *FEMS Microbiol. Ecol.* **76**, 576–591 (2011).
22. S. Bertilsson, O. Berglund, M. Pullin, S. Chisholm, *Vie Milieu* **55**, 225–232 (2005).
23. L. Aluwihare, D. Repeta, R. Chen, *Nature* **387**, 166–169 (1997).
24. A. Shibata, K. Kogure, I. Koike, K. Ohwada, *Mar. Ecol. Prog. Ser.* **155**, 303–307 (1997).
25. J. J. Grzymski, A. M. Dussaq, *ISME J.* **6**, 71–80 (2012).
26. D. Sher, J. W. Thompson, N. Kashtan, L. Croal, S. W. Chisholm, *ISME J.* **5**, 1125–1132 (2011).
27. J. J. Morris, Z. I. Johnson, M. J. Szul, M. Keller, E. R. Zinser, *PLOS ONE* **6**, e16805 (2011).
28. R. J. Parsons, M. Breitbart, M. W. Lomas, C. A. Carlson, *ISME J.* **6**, 273–284 (2012).
29. A. V. Klieve *et al.*, *Appl. Environ. Microbiol.* **71**, 4248–4253 (2005).
30. M. L. Wells, E. D. Goldberg, *Nature* **353**, 342–344 (1991).

Acknowledgments: We thank the members of the Chisholm laboratory, D. McLaughlin, and W. Burkholder for helpful discussions and advice; J. Jones for advice on particle analysis and providing access to equipment; N. Watson for microscopy assistance; and the J. King laboratory, Massachusetts Institute of Technology (MIT) for equipment use. J. Roden, L. Kelly, and P. Berube provided helpful suggestions on the manuscript. We also thank the captain and crew of the R/V Atlantic Explorer, R. Johnson, S. Bell, R. Parsons, and the rest of the BATS team for assistance with field sampling and providing access to data. Sequence data are available from the National Center for Biotechnology Information Sequence Read Archive (*Prochlorococcus* MED4 vesicles: SRP031649; field vesicles: SRP031871). This work was supported by grants from the Gordon and Betty Moore Foundation, the NSF Center for Microbial Oceanography: Research and Education (C-MORE), NSF-Biological Oceanography, and the MIT Energy Initiative Seed Grant program to S.W.C. F.S. and R.E.S. were supported by an award (NNA13AA90A) from the NASA Astrobiology Institute.

Supplementary Materials

www.sciencemag.org/content/343/6167/183/suppl/DC1
Materials and Methods
Supplementary Text
Figs. S1 to S13
Tables S1 to S6
References (*31*–*63*)

18 July 2013; accepted 25 November 2013
10.1126/science.1243457

Progenitor Outgrowth from the Niche in *Drosophila* Trachea Is Guided by FGF from Decaying Branches

Feng Chen[1,2,3] and Mark A. Krasnow[1,3]*

Although there has been progress identifying adult stem and progenitor cells and the signals that control their proliferation and differentiation, little is known about the substrates and signals that guide them out of their niche. By examining *Drosophila* tracheal outgrowth during metamorphosis, we show that progenitors follow a stereotyped path out of the niche, tracking along a subset of tracheal branches destined for destruction. The embryonic tracheal inducer *branchless* FGF (fibroblast growth factor) is expressed dynamically just ahead of progenitor outgrowth in decaying branches. Knockdown of *branchless* abrogates progenitor outgrowth, whereas misexpression redirects it. Thus, reactivation of an embryonic tracheal inducer in decaying branches directs outgrowth of progenitors that replace them. This explains how the structure of a newly generated tissue is coordinated with that of the old.

Many adult stem cells reside in specific anatomical locations, or niches, and are activated during tissue homeostasis and after injury (*1*–*4*). Although considerable effort has been made to identify factors that control stem cell proliferation and differentiation, how stem or progenitor cells move out of the niche and how they form new tissue are not well understood (*4*–*6*). Tissue formation in mature animals faces challenges not present in the embryo (*7*, *8*). The new cells migrate longer distances and navigate around and integrate into a complex milieu of differentiated tissues. In this work, we investigated the substratum and signals that guide *Drosophila* tracheal imaginal progenitor cells into the posterior during metamorphosis to form the pupal abdominal tracheae (PAT) that replace the posterior half of the larval tracheal system (tracheal metameres Tr6 to Tr10), which decays at this time (*9*, *10*) (Fig. 1A).

The PAT extend from the transverse connective (TC) branches in Tr4 and Tr5 (Fig. 1A). Each PAT consists of a multicellular stalk with many secondary branches, each of which has dozens of terminal cells that form numerous fine terminal branches (tracheoles) (*10*). There are two known tracheal progenitor populations at metamorphosis: dedifferentiated larval tracheal cells and spiracular branch (SB) imaginal tracheal cells set aside during embryonic tracheal

[1]Department of Biochemistry, Stanford University School of Medicine, Stanford, CA 94305–5307, USA. [2]Department of Genetics, Stanford University School of Medicine, Stanford, CA 94305–5307, USA. [3]Howard Hughes Medical Institute, Stanford University School of Medicine, Stanford, CA 94305–5307, USA.
*Corresponding author E-mail: krasnow@stanford.edu

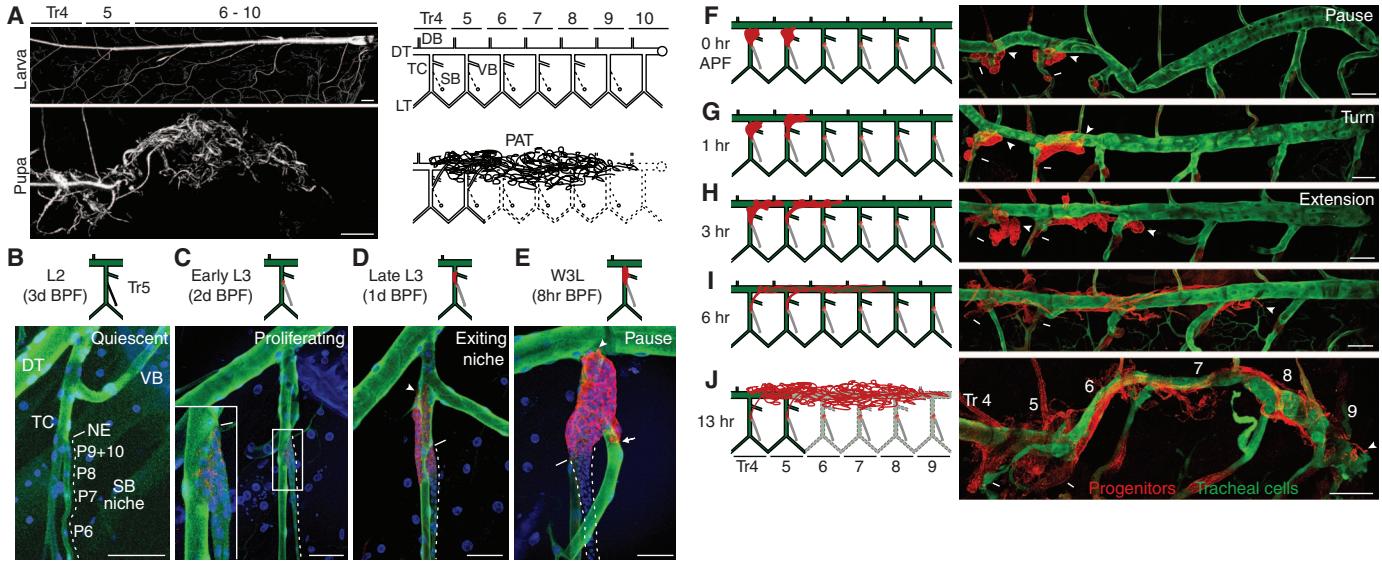

Fig. 1. Progenitor outgrowth during *Drosophila* tracheal metamorphosis. (**A**) Air-filled trachea (reflected light) (left) and schematics (right) in L3 larva and pupa ~13 hours after puparium formation. Tr, tracheal metamere; DB, dorsal branch; LT, lateral trunk; VB, visceral branch. Circles denote spiracles. Tracheal branches in the posterior (Tr6 to Tr10) are lost (dashed lines) during metamorphosis and are replaced by PAT from Tr4 and Tr5. (**B** to **E**) Fluorescence micrographs and schematics of Tr5 of *ppk4-Gal4>UAS-GFP; btl-RFP-moe* larva of the indicated ages stained to show activated tracheal progenitors (anti-RFP, red), larval tracheal cells (anti-GFP, green), and nuclei (4′,6-diamidino-2-phenylindole, blue). BPF, approximate time before puparium formation; W3L, wandering third-instar larva. (B) Quiescent progenitors in a Tr5 SB niche. Progenitors are also present in the SB niche of Tr2 to Tr4 and Tr6 to Tr9, but only those in Tr4 and Tr5 are activated to form PAT. P6 to P10, progenitors 6 to 10; the other five progenitors (P1 to P5) are shown in fig. S1A. NE, niche exit site (SB-TC junction). (C) Activated progenitors proliferating in the niche. (Inset) Progenitors near the niche exit site (dash), which have begun expressing *btl-RFP-moe* (red). (D) Progenitors exiting the niche. *btl-RFP-moe* expression increases and *ppk4>GFP* decreases as progenitors leave the niche and migrate dorsally along TC branches. Arrowhead, progenitor migration front. (E) Progenitors paused at the DT (arrowhead). Several progenitors have extended onto the VB (arrow). (**F** to **J**) Schematics and micrographs [as in (B) to (E)] of trachea (Tr4 to Tr9) of pupa of indicated ages APF. Paused progenitors (F) move onto the DT and turn posteriorly (G), extending along the DT (H and I) before ramifying into the PAT (J). Posterior tracheal branches start to collapse 9 hours APF and are fully collapsed and no longer conduct air by 13 hours APF. The larval cells die during metamorphosis (*10*), although we did not detect the apoptosis marker anticleaved caspase-3 during collapse (fig. S9). Scale bars: 100 μm, (A) and (F) to (J); 50 μm, (B) to (E).

development (*11*–*14*). Lineage tracing showed that PAT derive from imaginal progenitors (fig. S1, B and C).

To determine how progenitors in Tr4 and Tr5 reach the posterior, we used a *btl-RFP-moe* transgene (*15*) (RFP, red fluorescent protein) to label activated progenitor cells, and *ppk4>GFP* (*16*) (GFP, green fluorescent protein) to label larval tracheal branches (fig. S2A). Before metamorphosis, there are 7 to 10 quiescent progenitor cells in each SB niche (Fig. 1B and fig. S1A) (*11*, *13*). In early third larval instar (L3), progenitors proliferate but remain in the niche (Fig. 1C). Later in L3, progenitors leave the niche, moving onto the larval TC branches toward the dorsal trunk (DT) (Fig. 1D), while progenitors within the niche continue to proliferate (*13*). Progenitors in other metameres also proliferate but do not move out of the niche (fig. S2B). Migrating progenitors in Tr4 and Tr5 crawl along the basal surface of larval tracheal cells, with cytoplasmic projections emanating from cells at the leading edges of the progenitor cluster (fig. S3C). Progenitors maintain epithelial polarity and a lumen continuous with the SB and TC branches, forming a saclike structure (fig. S3, A and B) (*9*). By wandering L3, progenitors reach the DT (Fig. 1E), where they pause (~12 hours) until the onset of puparium formation (Fig. 1F).

Around 1 hour after puparium formation (APF), progenitors move onto the DT and turn posteriorly (Fig. 1G). Posterior migration continues for 9 hours, extending half the animal's length (~0.8 mm) past Tr9 (Fig. 1, H to J). Live imaging showed that progenitors move at ~1.7 μm/min, crawling along and wrapping around the DT as they migrate (movie S1).

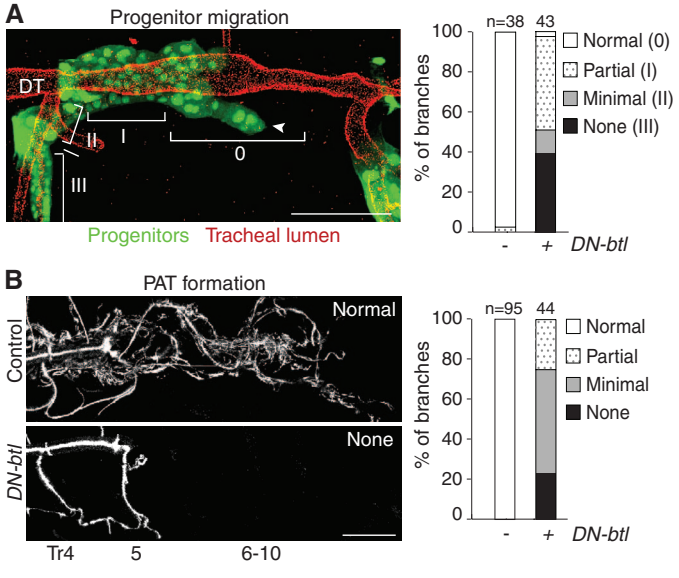

Fig. 2. Progenitor outgrowth requires *breathless* FGFR. (**A**) PAT progenitor migration in a control *esg^{P127}-Gal4, UAS-GFP/ act5c>Y>Gal4, UAS-GFP; UAS-FLP* pupa 6 hours APF at 18°C with progenitors marked with GFP (green) and tracheal lumens stained (red). Brackets show position of progenitor migration front in the four phenotypic classes (0, I, II, III) scored in control and in *esg^{P127}-Gal4, UAS-GFP/act5c>Y>Gal4, UAS-GFP; UAS-FLP/ UAS-DN-btl* pupae, in which dominant-negative *breathless* (*DN-btl*) is selectively expressed in progenitors. Examples of each phenotypic class can be found in fig. S5, A to D. Arrowhead, progenitor migration front. The graph at right shows quantification. n, number of branches. (**B**) PAT formation in control (top) and *DN-btl* pupae (bottom) as above, except reared for 1 to 2 additional days to allow formation of mature, air-filled pupal tracheae (reflected light). No PAT have formed in the *DN-btl* pupa. The graph shows quantification, with phenotypes classified as in fig. S5, E to H. Scale bars, 100 μm.

Differentiation begins as progenitors migrate. At the beginning of puparium formation (0 hours APF, Fig. 1F), a subset of progenitors that have exited the niche begins to express the terminal cell master regulator Pruned SRF (serum response factor) (*17*), initiating cell specialization (fig. S4A). As progenitors migrate along the DT, budlike structures composed of Pruned-expressing cells are detected at the tips of progenitor clusters, whereas Pruned-negative cells form the stalks of new trachea (fig. S4B). By 6 hours APF, Pruned-expressing progenitors in the tips adopt an elongated and differentiated morphology (fig. S4, C and D), flattening along the DT as they extend further posteriorly (movie S1). Around 13 hours APF, the PAT mature and fill with gas as posterior tracheal branches collapse (Fig. 1, A and J).

What guides tracheal progenitors on their stereotyped path along specific branches of the larval tracheal system? Expression of *breathless* (*btl*) FGFR (fibroblast growth factor receptor) is induced in PAT progenitors (*11*, *13*), as shown by the *btl-RFP-moe* reporter (Fig. 1, B to J). We tested whether the Btl pathway, which directs tracheal branch outgrowth in embryos (*18*–*20*) and larvae (*21*) and induces adult air-sac primordium formation (*22*), is involved. Expression of dominant-negative Btl FGFR (*19*) in the progenitors and their descendants (*23*) blocked migration and diminished or eliminated PAT formation (Fig. 2 and fig. S5). To determine the source of the only known Btl ligand, Branchless (Bnl) FGF (*20*), we used a *bnl* reporter, *bnl-Gal4* enhancer trap line NP2211 (*24*) driving *UAS-GFP*. Unlike previously described examples of tracheal outgrowth (*20*–*22*), *bnl* was not expressed in surrounding tissue. Instead, it was expressed within the tracheal system, specifically by larval tracheal cells along which progenitors migrate. The expression pattern is dynamic and precise, almost perfectly matching the positions and timing of progenitor migration (Fig. 3A and fig. S6A). In L3 animals, when progenitors are observed along the TC branches, *bnl>GFP* was expressed in TC larval cells in Tr4 and Tr5, but not in other metameres. Shortly after puparium formation, when PAT progenitors turn to migrate toward the posterior, DT larval cells in the segment just posterior to PAT

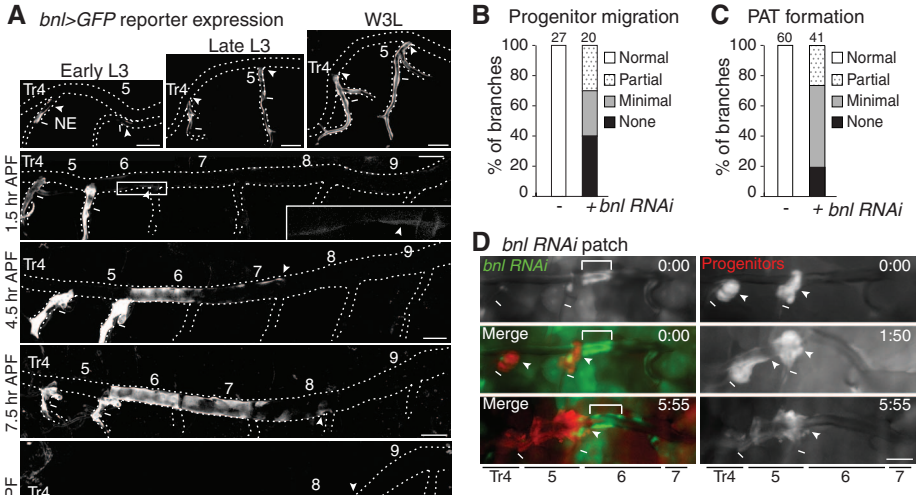

Fig. 3. Expression and requirement of *branchless* FGF during progenitor outgrowth. (**A**) *branchless* reporter expression during progenitor outgrowth visualized by GFP immunostaining (white) of *UAS-GFP; bnl-Gal4 NP2211/ btl-RFP-moe* larvae and pupae of indicated ages. Reporter expression dynamically expands along the progenitor outgrowth path, initially turning on in isolated larval cells in each area. Arrowheads denote furthest detected reporter expression. (**B** and **C**) Quantification (as in Fig. 2) of progenitor migration 3 hours APF (B) and PAT formation (C) phenotypes in control (*ppk4-Gal4, UAS-GFP; btl-RFP-moe*) and *ppk4-Gal4, UAS-GFP; btl-RFP-moe/ UAS-bnl RNAi* pupae, in which *bnl* was inactivated in larval tracheal cells. For examples of the phenotypic classes, see fig. S7, A and B. (**D**) Frames at indicated times (hours:minutes) APF from live imaging of an *act5c>Y>Gal4, UAS-GFP/ UAS-FLP; prd-Gal4, btl-RFP-moe/ UAS-bnl RNAi* pupa in which *bnl* expression was inactivated in a DT patch (brackets). Tr5 progenitors (*btl-RFP-moe*) exit the niche (dashes) and move onto the DT but never pass the patch. Scale bars, 100 μm.

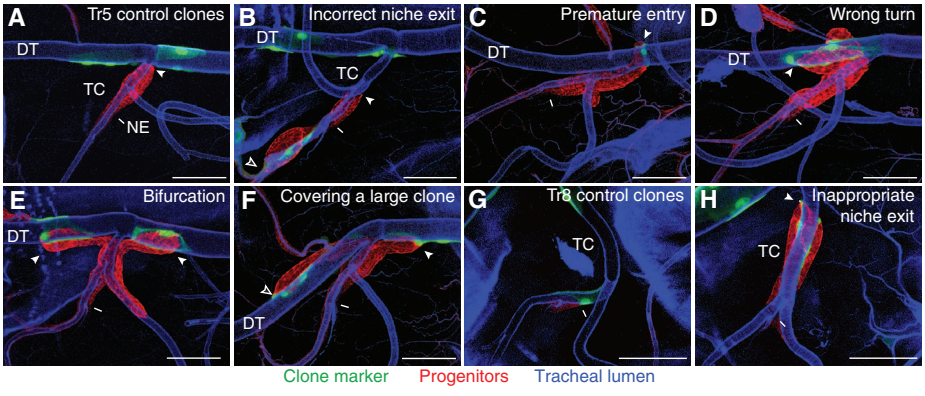

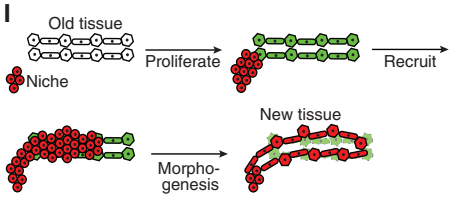

Fig. 4. Effect of ectopic *bnl* on progenitor migration. Tracheal progenitors (red, anti-RFP) in Tr4 or Tr5 [(**A**) to (**F**)] and Tr8 [(**G**) and (**H**)] of control (*dfr-FLP/ act5c>Y>Gal4, UAS-GFP; btl-RFP-moe*) and experimental (*dfr-FLP/ act5c>Y>Gal4, UAS-GFP; btl-RFP-moe/ UAS-bnl*) wandering third-instar larvae showing control clones of larval tracheal cells expressing GFP alone (green) [(A) and (G)] or experimental clones expressing GFP and ectopic *bnl* FGF [(B to F) and (H)]. Blue, tracheal lumen (Alexa Fluor 350-conjugated wheat germ agglutinin). Arrowheads denote progenitor migration fronts. (A) Progenitors have exited the niche and reached the TC-DT junction (arrowhead). Control clones (green) have no effect. (B) Some progenitors have exited the niche in the wrong direction along TC branches (open arrowhead), extending toward the *bnl*-expressing clone ventral to the niche exit. Other progenitors (solid arrowhead) have exited the niche normally toward DT. (C) Progenitors have prematurely moved onto DT, extending toward a single larval DT cell expressing *bnl*. (D) Inappropriate anterior migration of progenitors along DT (arrowhead) toward the *bnl*-expressing clone. (E) Bifurcation of progenitor cluster (arrowheads) toward a pair of *bnl*-expressing clones located anterior and posterior to the TC-DT junction. (F) Bifurcation (arrowheads) where progenitors extend to fill the shape of a large *bnl*-expressing clone (open arrowhead). (G) Progenitors in Tr8 (as well as Tr3 and Tr6 to Tr9) normally remain within the niche and are unaffected by control clones. (H) Tr8 progenitors exit the niche toward a clone of *bnl*-expressing cells on TC branches. Scale bars [(A) to (H)], 100 μm. (**I**) Model of progenitor outgrowth guided by a signal produced by decaying tissue (green). Progenitors (red) are attracted to and form new tissue at the site of decay.

progenitors express *bnl>GFP*. As progenitors continue along the DT, DT larval cells activate *bnl>GFP* expression one segment at a time from anterior to posterior, matching progenitor movement.

This dynamic *bnl* expression along the migration path is required for progenitor outgrowth. Knockdown of *bnl* expression by RNA interference (RNAi) in larval tracheal cells blocked migration and resulted in diminished or absent PAT (Fig. 3, B and C; fig. S7, A to C; and movie S2). Mosaic expression of *bnl RNAi* in small patches along the path (*23*) also arrested migration, so long as the patch encompassed the full DT circumference (Fig. 3D; fig. S7, D and E; and movies S3 and S4). Thus, Bnl is required all along the migration path, and the signal does not cross even short gaps.

Ectopic *bnl* expression in GFP-labeled clones of larval tracheal cells induced by *dfr-FLP* (*23*) redirected progenitor migration. Depending on the location of the clones, ectopic *bnl* caused incorrect exit from the niche, premature entry onto the DT, or wrong turns on the DT (Fig. 4, B to D). Dual clones induced bifurcation with groups of progenitors moving toward each ectopic *bnl* source (Fig. 4E). Clones in Tr3 and posterior metameres caused progenitors in these regions to leave the niche, even though they do not normally do so (Fig. 4, G and H, and fig. S8, D and E). When there was a large clone, progenitors migrated throughout the clone (Fig. 4F), implying that progenitors do not require a gradient and will spread to cover an entire region of cells expressing *bnl* at equivalent levels. When *bnl*-expressing clones failed to induce migration, the clones appeared to be too far from the progenitors or there was competition from another clone close by (fig. S8, A and B). Ectopic *bnl* expression within the progenitor cluster arrested migration (fig. S8C).

The results show that the embryonic tracheal inducer Bnl FGF guides tracheal progenitors out of the niche and into the posterior during tracheal metamorphosis. The source of Bnl is the larval tracheal branches destined for destruction, which serve both as the source of the chemoattractant and as the substratum for progenitor migration. Several days earlier in embryos, these larval tracheal branches were themselves induced by Bnl provided by neighboring tissues. But after embryonic development, most tracheal cells, including those in the decaying larval branches, downregulate *btl* FGFR expression (fig. S2A) and thus do not respond to (or sequester) the Bnl signal they later express. One of the most notable aspects of this larval Bnl is its exquisitely specific pattern in decaying larval branches, which presages progenitor outgrowth. It is unclear how Bnl expression is controlled, though it does not appear to require signals from migrating progenitors because the *bnl* reporter expression front progressed normally when progenitor outgrowth was stalled by a tracheal break (fig. S6C). Perhaps expression of Bnl involves gradients in the tracheal system or spatial patterning cues established during embryonic development in conjunction with temporal signals mediated by molting hormones.

Because the signal guiding progenitor migration is provided by tracheae destined for destruction, progenitors become positioned along the larval branches they replace (Fig. 4I). Perhaps during tissue repair and homeostasis, recruitment of adult stem or progenitor cells from the niche is similarly guided by signals from decaying tissue, thereby ensuring that new tissue is directed to the appropriate sites.

References and Notes

1. N. Barker, S. Bartfeld, H. Clevers, *Cell Stem Cell* **7**, 656–670 (2010).
2. G. B. Adams, D. T. Scadden, *Nat. Immunol.* **7**, 333–337 (2006).
3. A. Alvarez-Buylla, D. A. Lim, *Neuron* **41**, 683–686 (2004).
4. C. Blanpain, E. Fuchs, *Nat. Rev. Mol. Cell Biol.* **10**, 207–217 (2009).
5. E. Sancho, E. Batlle, H. Clevers, *Curr. Opin. Cell Biol.* **15**, 763–770 (2003).
6. G. L. Ming, H. Song, *Neuron* **70**, 687–702 (2011).
7. E. Nacu, E. M. Tanaka, *Annu. Rev. Cell Dev. Biol.* **27**, 409–440 (2011).
8. K. D. Poss, *Nat. Rev. Genet.* **11**, 710–722 (2010).
9. T. Matsuno, *Jap. J. Appl. Entomol. Zool.* **34**, 165–167 (1990).
10. G. Manning, M. A. Krasnow, in *The Development of* Drosophila melanogaster, M. Bate, A. Martinez-Arias, Eds. (Cold Spring Harbor Laboratory Press, Woodbury, NY, 1993), vol. 1, pp. 609–685.
11. M. Weaver, M. A. Krasnow, *Science* **321**, 1496–1499 (2008).
12. A. Guha, L. Lin, T. B. Kornberg, *Proc. Natl. Acad. Sci. U.S.A.* **105**, 10832–10836 (2008).
13. C. Pitsouli, N. Perrimon, *Development* **137**, 3615–3624 (2010).
14. M. Sato, Y. Kitada, T. Tabata, *Dev. Biol.* **318**, 247–257 (2008).
15. C. Ribeiro, M. Neumann, M. Affolter, *Curr. Biol.* **14**, 2197–2207 (2004).
16. L. Liu, W. A. Johnson, M. J. Welsh, *Proc. Natl. Acad. Sci. U.S.A.* **100**, 2128–2133 (2003).
17. K. Guillemin *et al.*, *Development* **122**, 1353–1362 (1996).
18. C. Klämbt, L. Glazer, B. Z. Shilo, *Genes Dev.* **6**, 1668–1678 (1992).
19. M. Reichman-Fried, B. Z. Shilo, *Mech. Dev.* **52**, 265–273 (1995).
20. D. Sutherland, C. Samakovlis, M. A. Krasnow, *Cell* **87**, 1091–1101 (1996).
21. J. Jarecki, E. Johnson, M. A. Krasnow, *Cell* **99**, 211–220 (1999).
22. M. Sato, T. B. Kornberg, *Dev. Cell* **3**, 195–207 (2002).
23. Materials and methods are available as supporting material on *Science* Online.
24. S. Hayashi *et al.*, *Genesis* **34**, 58–61 (2002).

Acknowledgments: We thank M. Weaver, M. Metzstein, and other lab members for advice and reagents. This work was supported by a Genentech Graduate Fellowship and a Ruth L. Kirschstein NIH training grant (F.C.) and the Howard Hughes Medical Institute.

Supplementary Materials

www.sciencemag.org/content/343/6167/186/suppl/DC1
Materials and Methods
Figs. S1 to S10
References (*25*–*39*)
Movies S1 to S4

4 June 2013; accepted 12 November 2013
10.1126/science.1241442

Mutational Analysis Reveals the Origin and Therapy-Driven Evolution of Recurrent Glioma

Brett E. Johnson,[1]* Tali Mazor,[1]* Chibo Hong,[1] Michael Barnes,[2] Koki Aihara,[3,4] Cory Y. McLean,[1]† Shaun D. Fouse,[1] Shogo Yamamoto,[3] Hiroki Ueda,[3] Kenji Tatsuno,[3] Saurabh Asthana,[5,6] Llewellyn E. Jalbert,[7] Sarah J. Nelson,[7,8] Andrew W. Bollen,[2] W. Clay Gustafson,[9] Elise Charron,[10] William A. Weiss,[1,9,10] Ivan V. Smirnov,[1] Jun S. Song,[11,12] Adam B. Olshen,[6,11] Soonmee Cha,[1] Yongjun Zhao,[13] Richard A. Moore,[13] Andrew J. Mungall,[13] Steven J. M. Jones,[13] Martin Hirst,[13] Marco A. Marra,[13] Nobuhito Saito,[4] Hiroyuki Aburatani,[3] Akitake Mukasa,[4] Mitchel S. Berger,[1] Susan M. Chang,[1] Barry S. Taylor,[5,6,11]‡ Joseph F. Costello[1]‡

Tumor recurrence is a leading cause of cancer mortality. Therapies for recurrent disease may fail, at least in part, because the genomic alterations driving the growth of recurrences are distinct from those in the initial tumor. To explore this hypothesis, we sequenced the exomes of 23 initial low-grade gliomas and recurrent tumors resected from the same patients. In 43% of cases, at least half of the mutations in the initial tumor were undetected at recurrence, including driver mutations in *TP53*, *ATRX*, *SMARCA4*, and *BRAF*; this suggests that recurrent tumors are often seeded by cells derived from the initial tumor at a very early stage of their evolution. Notably, tumors from 6 of 10 patients treated with the chemotherapeutic drug temozolomide (TMZ) followed an alternative evolutionary path to high-grade glioma. At recurrence, these tumors were hypermutated and harbored driver mutations in the RB (retinoblastoma) and Akt-mTOR (mammalian target of rapamycin) pathways that bore the signature of TMZ-induced mutagenesis.

The genetic landscape of tumors is continually evolving, which can be an impediment to the clinical management of cancer patients with recurrent disease (*1*, *2*). In contrast to the clonal evolution of hematological malignancies (*3*, *4*) and solid tumor metastases (*5*–*7*), the local regrowth of solid tumors after surgery occurs under a unique set of evolutionary pressures, which are further affected by adjuvant therapies. Through the acquisition of new mutations, residual tumor cells can progress to a more aggressive state. Grade II astrocytic gliomas are

Supplementary Materials for

Progenitor Outgrowth from the Niche in *Drosophila* Trachea Is Guided by FGF from Decaying Branches

Feng Chen and Mark A. Krasnow*

*Corresponding author E-mail: krasnow@stanford.edu

Published 10 January 2014, *Science* **343**, 186 (2014)
DOI: 10.1126/science.1241442

This PDF file includes:

Other Supplementary Material for this manuscript includes the following:
(available at www.sciencemag.org/content/343/6167/186/suppl/DC1)

Supporting Online Material

Materials and methods

Drosophila strains and reporter lines

*btl-RFP-mo*e (gift from M. Affolter, Biozentrum University of Basel) is a transgene that expresses an RFP-moesin fusion protein under the control of a *btl* enhancer element (*15*). Line CB02854 (*25*) (Flytrap, Yale University) contains a GFP enhancer trap insertion at the *bnl* locus. The Gal4-UAS system (*26*) was used to express fluorescent reporters, other proteins, and RNAi transgenes in specific tissues and cell types *in vivo*. Gal4 drivers were: *ppk4-Gal4* (*16*) (gift from L. Liu, Peking University) a transgene containing 2 kb of the *ppk4* promoter region controlling *Gal4* and expressed in all larval tracheal cells; *esg^{P127}-Gal4 (11, 27, 28)*, an enhancer trap at the *escargot* locus expressed in all imaginal progenitor cells and tracheal fusion cells; *prd-Gal4* (*29*), a transgene expressing *Gal4* in the *paired* pair-rule gene pattern; and Gal4 enhancer trap lines NP2211 and NP3520 (Drosophila Genetic Resource Center; Kyoto Institute of Technology) (*24*) with insertions at the *bnl* locus. UAS responders were: *UAS-GFP (29)*, *UAS-FLP122 (29)*, *UAS-DN-btl* (*19*), *UAS-bnl-RNAi* GD5730 and *UAS-btl-RNAi* GD948 (*30*) (Vienna Drosophila RNAi Center), *UAS-bnl-A1-1* (*31*), and *UAS-rpr (29)*. *tub-Gal80ts (29)*, a transgene that ubiquitously expresses a temperature-sensitive conditional repressor of GAL4, was used to limit UAS responder expression to specific time periods. The FLP recombinase system (*32*) was used for permanent marking of tissues and cells and lineage labeling. *dfr-FLP* (M. Metzstein and M.A.K., unpublished) is a transgene with a multimerized tracheal-specific *dfr* enhancer element (*33*) cloned upstream of an *hsp70* minimal promoter driving expression of FLP. *act5c>Y>Gal4 (34)*, a ubiquitously expressed FLP-dependent transgene in which Gal4 is expressed following FLP-mediated recombination, was used for FLP-out experiments (see below). Crumbs::GFP (Crb::GFP-A) (gift from Y. Hong, University of Pittsburgh School of Medicine) encodes a functional Crumbs-GFP fusion protein knocked into the endogenous *crumbs* locus (*35*), which labels the apical epithelial surface and tracheal lumen. All crosses were carried out at 25˚C unless otherwise indicated.

Lineage trace and FLP-out experiments

All lineage trace and FLP-out experiments used *act5c>Y>Gal4, UAS-GFP* and a *FLP* transgene. Expression of FLP recombinase catalyzes "FLP-out" (removal) of a stop cassette and thereby activation of the *act5c>Y>Gal4* transgene (*34*), which then expresses Gal4 that drives expression of *UAS-GFP*, to permanently label the cells in which recombination has occurred and their progeny, and expression of other UAS responders as indicated.

esg^{P127}-Gal4 (11, 27, 28) is expressed in imaginal cells, including the SB tracheal progenitors, and fusion cells of the tracheal system. FLP-out experiments with a *Drosophila* strain carrying *esg^{P127}-Gal4* and *UAS-FLP* transgenes crossed to the *act5c>Y>Gal4, UAS-GFP* strain permanently labels imaginal cells and their progeny (*11*). Larval tracheal cells were also sporadically labeled, but because rearing the animals at 18°C reduced this unwanted labeling, all crosses and FLP-out experiments with *esg^{P127}-Gal4* were conducted at 18°C.

drifter (*dfr)/ ventral veins lacking* (*vvl*) is a transcription factor expressed in tracheal cells during embryonic development (*36*). In *dfr-FLP*; *act5c>Y>Gal4, UAS-GFP* animals raised at 25°C, GFP was expressed in larval tracheal clones that covered approximately 30 to 80% of the trachea. Animals raised at lower temperature had larger clones. To knockdown *bnl* in tracheal clones that encompassed the full circumference of the DT, *dfr-FLP/ act5c>Y>Gal4,*

UAS-GFP; btl-RFP-moe/ UAS-bnl RNAi animals were raised at 21°C. *dfr-FLP/ act5c>Y>Gal4, UAS-GFP; btl-RFP-moe/ UAS-bnl* animals raised at 25°C expressing ectopic Bnl (*UAS-bnl-A1-1*) in tracheal clones were viable and survived beyond puparium formation; the animals had slight defects in the shape and spacing of the larval branches and had local tufts of tracheoles, but the overall structure of the larval tracheal system was unaffected (fig. S10).

FLP-out experiments with the *prd-Gal4* driver in *act5c>Y>Gal4, UAS-GFP/ UAS-FLP; prd-Gal4, btl-RFP-moe/ UAS-bnl RNAi* animals labeled alternating segments of the epidermis and predominantly labeled alternating segments of the trachea.

Larval and pupal staging

L2 larvae were distinguished from L3 larvae by appearance of anterior spiracles. The relative ages of L3 larvae were inferred from the size of the animal; older larvae are larger. Wandering third instar larvae (W3L) and newly formed pupae (0 hr APF) were identified as described (*37*). 0 hr APF animals were selected and subsequent time points were determined by hours elapsed since selection.

Antibody and tracheal stains

Larvae and pupae were dissected by ventral filleting and fixed in 4% paraformaldehyde for 30 minutes then immunostained as described (*38*). GFP and RFP signals were amplified by immunostaining with polyclonal chicken anti-GFP (Abcam, ab13970; used at 1:1000) and polyclonal rabbit anti-DsRED (Clontech #632496; 1:300) primary antibodies. Pruned (dSRF) protein was detected with mAb2-161, a monoclonal mouse anti-dSRF antibody (used at 1:200) (*39*). A monoclonal rabbit anti-cleaved Caspase-3 antibody (Cell Signaling #9664) was used to detect apoptotic cells. Secondary antibodies used were: DyLight649-conjugated donkey-anti-chicken, DyLight649-conjugated donkey-anti-rabbit, Cy5-conjugated goat-anti-mouse (Jackson Immunoresearch), Alexa488-conjugated goat-anti-chicken and Alexa555-conjugated goat-anti-rabbit (Invitrogen). Tracheal lumens were stained with Alexa Fluor 350-conjugated or tetramethylrhodamine-conjugated wheat germ agglutinin (WGA) (Invitrogen; 1:1000) and with a rhodamine-conjugated chitin-binding probe (NEB; 1:300) for 1 hour at room temperature. Nuclei were stained with 4',6-Diamidino-2-Phenylindole, Dihydrochloride (DAPI) (Molecular Probes). Cuticle that lines larval tracheae autofluoresces and was also detected in the DAPI channel. Specimens were analyzed and digital images captured on confocal (Leica SP2 AOBS) and conventional florescence (Zeiss Axiophot and Leica MZ16 FA) microscopes. Air-filled tracheae were visualized on the Leica SP2 AOBS by reflected light. Unless otherwise indicated, all fluorescent micrographs are maximum projections of the confocal stack.

Live imaging progenitor migration

Immobile white *btl-RFP-moe* pupae (0 hr APF) were cleaned with a damp tissue and placed within a drop of halocarbon oil on a 6 cm Petri dish. Pupae were positioned with forceps for optimal imaging of tracheal progenitors in Tr4 and Tr5. Movies were acquired on a Zeiss Axio Observer.Z1 inverted microscope equipped with a XL multi S1 incubator to maintain temperature at 25˚C. Images were acquired every 3 - 5 minutes for up to 7 hours, after which the RFP signal from the *btl-RFP-moe* reporter diminishes. Image capture times were limited to 0.5 sec or less to minimize phototoxicity.

Monitoring *bnl* expression with *bnl* reporter lines

Because it proved difficult to obtain reliable signals for *bnl* expression by *in situ* hybridization or immunostaining for Bnl protein during metamorphosis, we used Gal4 enhancer trap lines NP2211 and NP3520 and GFP enhancer trap line CB02854 with insertions at the *bnl* locus within a 300 bp region 5' to the *bnl* transcription start site to monitor *bnl* expression during metamorphosis. All three enhancer trap reporters showed dynamic expression all along the route of PAT progenitor migration, with the exception noted below. CB02854 reported slightly earlier expression along the DT than NP2211 and NP3520, presumably because the binary Gal4/UAS system introduces a delay due to translation of Gal4 and induction of the GFP reporter. No expression of these reporters was detected in the section of DT between the Tr4 and Tr5 TC branches (the Tr5 DT), along which the Tr4 SB progenitors migrate to reach the next section of DT where they meet the progenitors from the Tr5 SB and continue migrating posteriorly along the DT. We infer that this part of the endogenous *bnl* expression pattern has a separate enhancer not reported by these enhancer trap lines because *bnl* RNAi knockdown in this region blocked Tr4 progenitor migration (fig. S7D; Movie S4).

Supplementary Figures

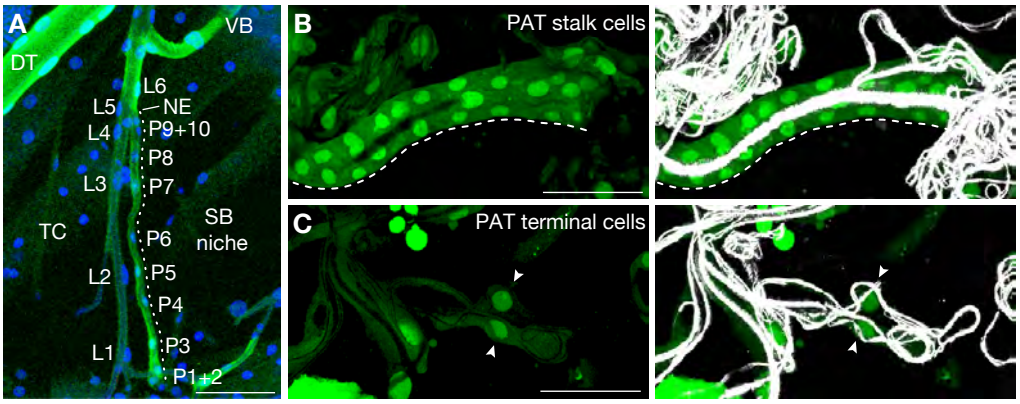

Figure S1. Visualizing and lineage-tracing tracheal progenitors that migrate out of the spiracular branch niche. **(A)** Cells in the Tr5 spiracular branch (SB) niche (dotted line) before progenitor activation. A portion of tracheal metamere Tr5 is shown from a *ppk4>GFP; btl-RFP-moe* second instar larva (L2) stained for GFP to show tracheal cells (green), for RFP to show activated progenitors (red), and labeled with DAPI to show cell nuclei (blue). The 10 progenitor cells (P1 - P10) in the spiracular branch (SB) niche are labeled, as are six larval tracheal cells (L1-L6) in the neighboring transverse connective (TC). Progenitors P9 and P10 connect to L5 and L6 and the rest of the larval tracheal system at the SB-TC junction, which we refer to as the niche exit (NE) and indicate with a dash. P1 and P2 connect to the epidermis. Progenitors in tracheal metameres Tr2 - Tr4 and Tr6 - Tr9 (not shown) appear similar. DT, dorsal trunk; VB, visceral branch. **(B, C)** *escargot>FLP* lineage trace showing imaginal progenitors give rise to pupal abdominal trachea (PAT). Fluorescent micrographs of differentiated PAT stalk (B) and terminal (C) cells in an *esg^{P127}-Gal4, UAS-GFP/act5c>Y>Gal4, UAS-GFP; UAS-FLP* pupa approximately 24 hr after puparium formation (APF) at 18ºC. SB and other *esg^{P127}*-lineage (imaginal) progenitors and their descendants are labeled with GFP (green), and air-filled tracheae and terminal branches (tracheoles) are visualized by reflected light (white). Dashed line, PAT stalk; arrowheads, individual terminal cells, each of which has formed many tracheoles. Bars, 50 µm.

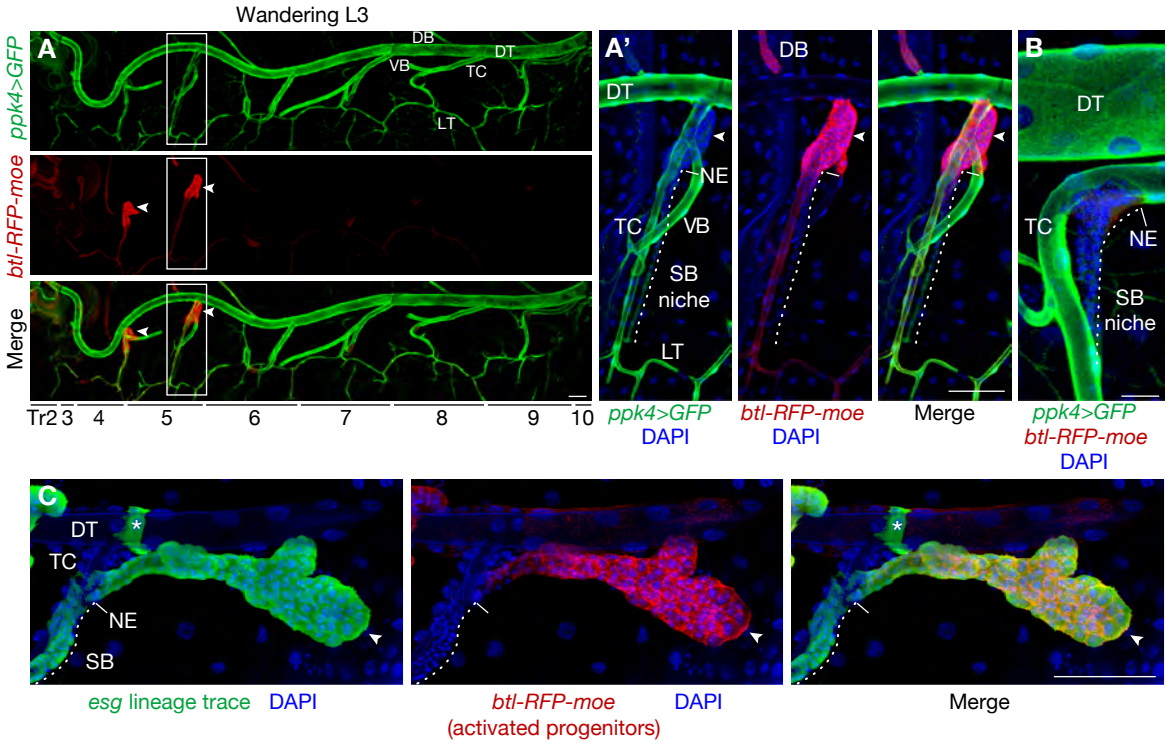

Figure S2. Selective expression of a *breathless* FGFR reporter in outgrowing progenitors. (A) Fluorescent micrograph of a *ppk4>GFP; btl-RFP-moe* wandering third instar (W3L) larva stained for GFP to show *ppk4>GFP* expression and for RFP to show *btl-RFP-moe* expression as in Fig. 1E. Close-ups of metamere Tr5 (boxed) are shown in **A'**, with nuclei stained with DAPI (blue). Note that larval tracheal cells along the dorsal trunk (DT), transverse connectives (TC), lateral trunk (LT), visceral branch (VB) and posterior (Tr6 to Tr10) dorsal branches (DB) express *ppk4>GFP* but little or no *btl-RFP-moe*, which must have been downregulated after embryonic development *(15)*. Conversely, progenitors have turned off the *ppk4>GFP* reporter, and Tr4 and Tr5 progenitors that are exiting the niche (arrowheads) highly express the *btl* reporter. Dotted lines, SB niche. Dashes, SB niche exit (NE). De-differentiating cells in anterior (Tr2 to Tr5) dorsal branches (DB) *(11)* also express the *btl-RFP-moe* reporter (A') though at lower levels. **(B)** Posterior SB niche after progenitor activation. A portion of tracheal metamere Tr9 of the larva in A is shown with nuclei stained with DAPI (blue). Progenitors have proliferated and those near the niche exit express low but detectable *btl-RFP-moe* (red). However, progenitors do not exit the niche, as they do in Tr4 and Tr5. **(C)** Close up of progenitors growing out of the SB niche in an *esg^{P127}-Gal4, UAS-GFP/act5c>Y>Gal4, UAS-GFP; UAS-FLP/ btl-RFP-moe* pupa 6 hr APF at 18ºC stained for *esg^{P127}* lineage-trace progenitors (anti-GFP, green), activated progenitors (anti-RFP, red), and nuclei (DAPI, blue). Note that all progenitors that have exited the SB niche (arrowheads) express the *btl* reporter but those still in the niche (dotted line) do not. *, larval fusion cells that also express *esg*. Dash, SB niche exit (NE). Bars, 100 µm (A, C) and 25 µm (B).

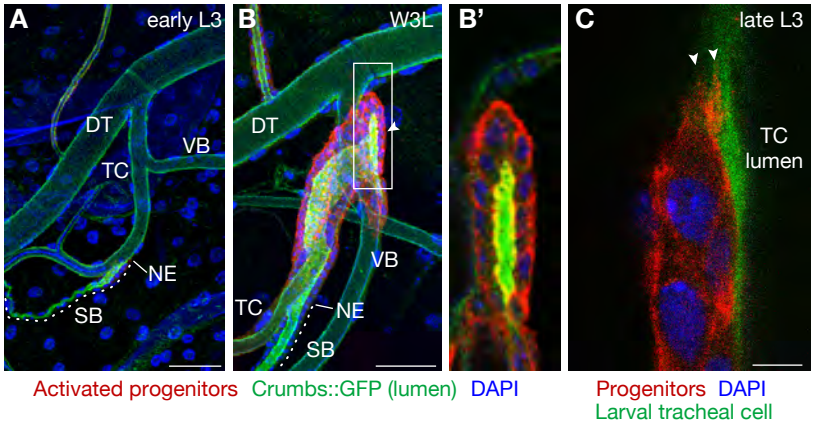

Figure S3. Progenitor outgrowth morphology. Portion of tracheal metamere Tr4 in *btl-RFP-moe/ crumbs::GFP* early third-instar (L3) **(A)** and wandering third instar (W3L) **(B)** larvae stained for activated tracheal progenitors (anti-RFP, red) and apical tracheal surface and lumen (anti-GFP, green). In early L3 larvae (A), the SB contains a lumen and forms a junction with the larval transverse connective (TC) at the niche exit (NE) site. In wandering L3 larvae (B), the outgrowing progenitors have formed a monolayer-epithelial sac extending from the SB niche (arrowhead). The lumen of the expanding progenitor sac is continuous with the SB lumen and larval TC at the NE. Inset **(B')** shows an optical z-section of the boxed region. Note Crumbs::GFP and RFP-moesin co-localization on apical progenitor cell surfaces. **(C)** Close-up of migrating progenitors in Fig. 1D. Progenitors migrate on the basal surface of larval tracheal cells; cytoplasmic extensions emanate from the leading progenitors (arrowheads), indicating active migration. Bars, 50 µm (A, B) and 5 µm (C).

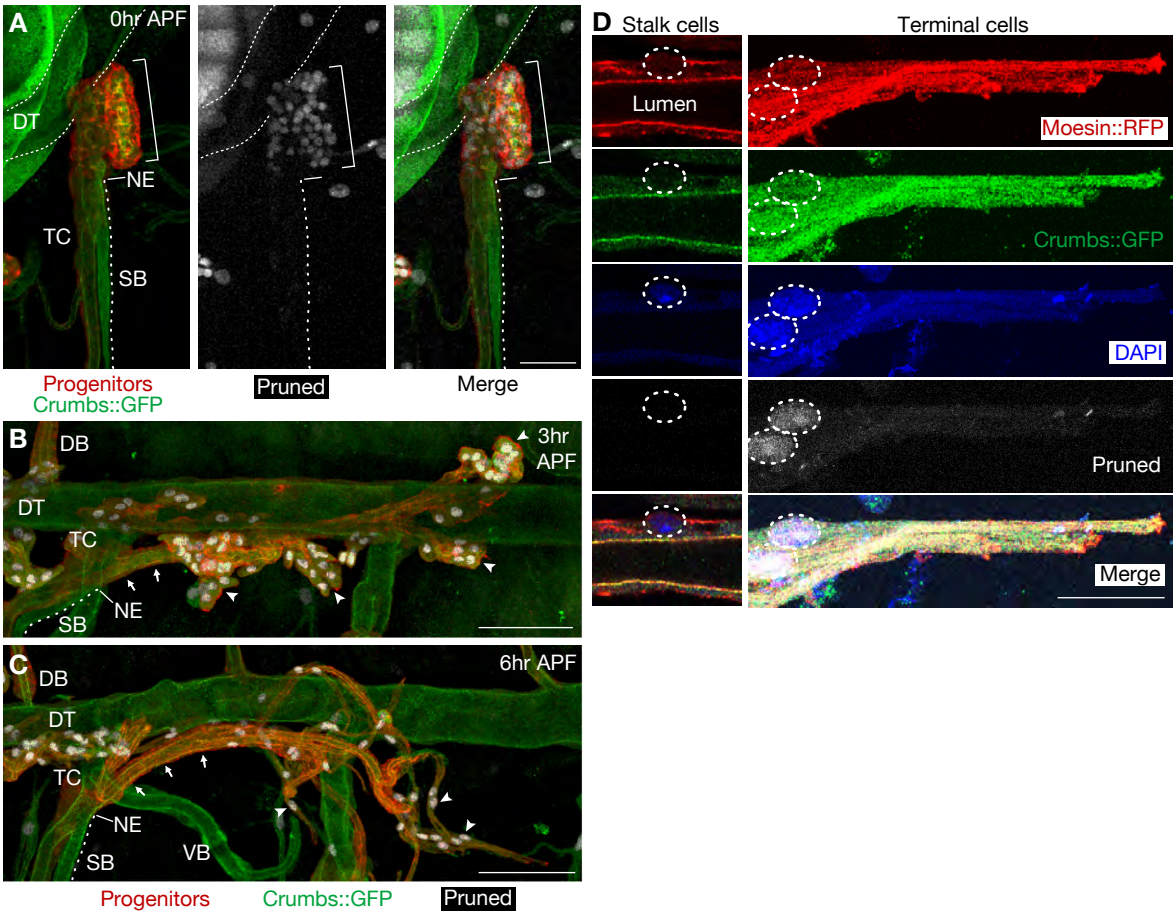

Figure S4. Migrating progenitors initiate the tracheal morphogenesis program. (A) Portion of tracheal metamere Tr5 in *btl-RFP-moe/ crumbs::GFP* larva at onset of puparium formation (0 hr APF) stained for Pruned SRF (white), tracheal progenitors (anti-RFP, red), and apical surfaces of tracheae (anti-GFP, green). Note that a subset of progenitors in the outgrowing cluster (bracket) has initiated the terminal cell differentiation program as indicated by expression of Pruned. Dotted line, SB niche; dash, SB niche exit (NE). **(B, C)** Pupae as above at 3 hr (B) and 6 hr (C) APF. Pruned-expressing progenitors are segregated at the tips of the outgrowing PAT (arrowheads), while Pruned-negative cells form the PAT stalk (arrows). **(D)** Close-up of PAT stalk and terminal cells of the pupa in C also stained for DAPI to show nuclei. Note terminal cells have elongated morphology and have formed intracellular lumens (tracheoles) (outlined by RFP-moesin and Crumbs::GFP) whereas progenitors in the stalk do not express Pruned, do not form tracheoles, and have apical Crumbs::GFP localization. Bars, 50 µm (A), 100 µm (B, C), 25 µm (D).

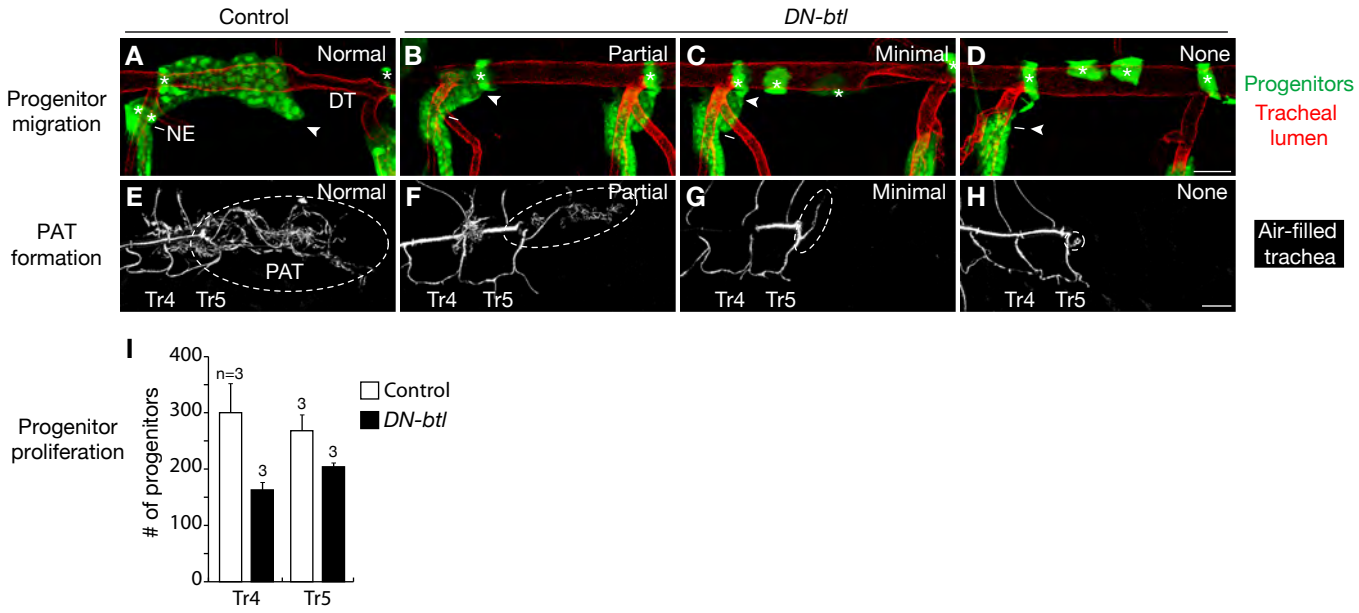

Figure S5. Effect of dominant negative Breathless on progenitor migration, proliferation, and PAT formation. Dominant-negative *breathless* (*DN-btl*) was expressed in SB tracheal progenitors and their progeny, and the animals were analyzed 6 hr APF at 18ºC for effects on Tr4 and Tr5 progenitor migration (A-D) as described in Fig. 2A, or for effects on progenitor proliferation by counting the number of progenitors (I), or animals were reared for an additional 1 to 2 days to allow PAT formation (E-H). **(A-D)** Examples of progenitor migration phenotypes. (A) Normal (Class 0), migration similar to that in control pupae. (B) Partial (Class I), reduced migration along DT. (C) Minimal (Class II), no migration along DT. (D) None (Class III), progenitors do not exit SB niche. Progenitors, green (GFP fluorescence); larval tracheal branches, red (rhodamine-conjugated WGA and rhodamine-conjugated chitin-binding protein); dash, niche exit (NE); *, larval tracheal fusion cells and sporadic larval tracheal cells that also express the progenitor lineage label. **(E-H)** Examples of PAT formation phenotypes. (E) Normal, extensive PAT formation similar to that in controls. (F) Partial, reduced PAT ramification and extension into posterior. (G) Minimal, limited PAT formation and extension with thin branches at PAT base. (H) None, no PAT formation. White, mature air-filled pupal tracheae; dashed ovals, extent of PAT formation. Similar though less severe progenitor migration and PAT formation phenotypes were observed with expression of a *btl RNAi* transgene. **(I)** Quantification of cell number in Tr4 and Tr5 SB niches. The 10 SB progenitors (fig. S1A) proliferate extensively in both control and *DN-btl*-expressing pupae, but note there are fewer cells in the *DN-btl* pupae, in which progenitors do not leave the niche. Bars, 50 µm (A-D), 100 µm (E-H).

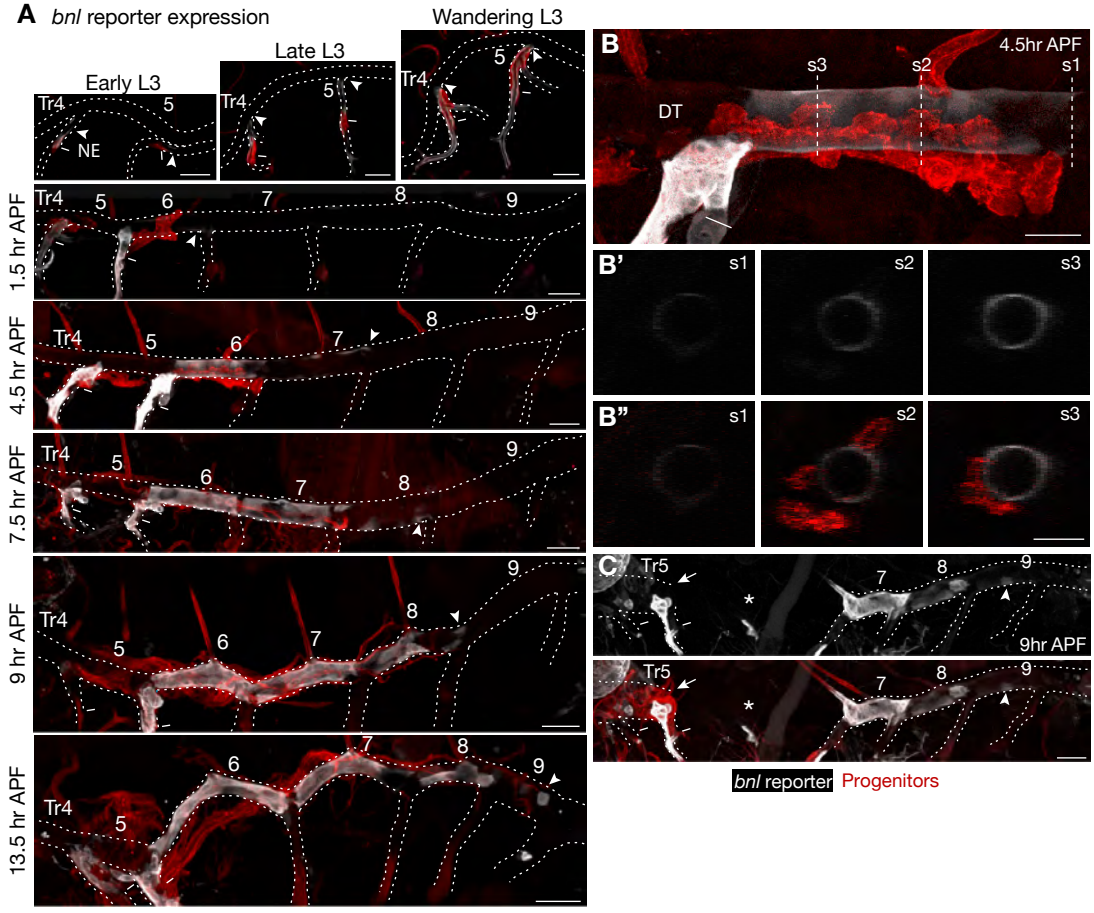

Figure S6. Expression of *branchless (bnl)* just ahead of migrating tracheal progenitors. (A) *bnl-Gal4 NP2211/ UAS-GFP; btl-RFP-moe* animals of the indicated ages showing *bnl* reporter expression (GFP immunostain, white) as in Fig. 3A but co-stained to show relationship to migrating progenitors (RFP immunostain, red). Isolated larval cells initiate *bnl* reporter expression (arrowheads) ahead of migrating progenitors. Note reporter expression in TC cells ventral to the niche exit that is ignored by migrating progenitors, and absence of reporter expression in the Tr5 DT, along which Tr4 progenitors migrate to meet Tr5 progenitors. Dashes, niche exit (NE). **(B)** Close up of Tr6 in pupa 4.5 hr APF. Optical sections through dorsal trunk (DT) at planes indicated (s1, s2, s3) are shown in **B'** and **B''** (*bnl* reporter expression, white; migrating progenitors, red). Although *bnl* reporter expression initially appears in individual DT cells (section s1), it expands to cover the entire circumference of the DT (section s3). However, progenitors do not completely envelop the entire circumference (section s3). **(C)** A 9 hr APF pupa, stained as above, with sporadic break that has separated DT into anterior and posterior regions. Note that progenitors (red, arrow) have not migrated beyond the lesion (*) but *bnl* reporter expression has expanded beyond lesion into posterior metameres (arrowhead) just as in animals with intact DT (panel A). Bars, 100 µm (A,C), 50 µm (B).

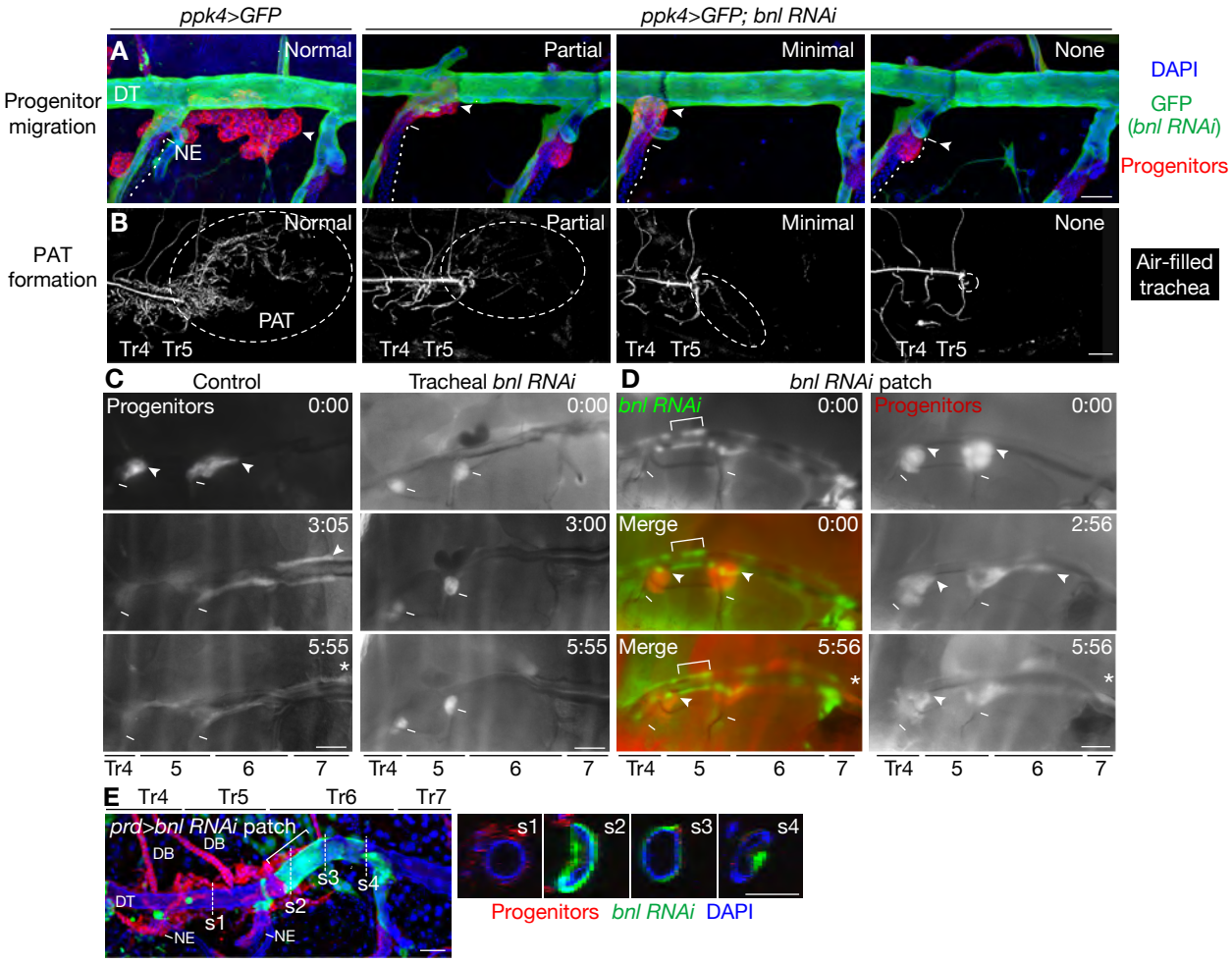

Figure S7. Progenitor migration and PAT formation phenotypes from *branchless (bnl)* knockdown along migration route. (A) Progenitor migration in a control (*ppk4-Gal4/ UAS-GFP; btl-RFP-moe*) and *ppk4-Gal4/ UAS-GFP; btl-RFP-moe/ UAS-bnl RNAi* pupa in which *bnl RNAi* was expressed in all larval tracheal cells. The effect on progenitor migration 3 hr APF was analyzed as described in Fig. 2A after staining for progenitors (anti-RFP, red), larval tracheal cells in which *bnl* is knocked down by RNAi (anti-GFP, green), and nuclei (DAPI, blue). Examples of migration phenotypes are indicated, classified as in fig. S5A-D. Dotted line, SB niche; dash, niche exit (NE); arrowheads, extent of progenitor migration. **(B)** Pupae as in A reared for another 1 to 2 days to allow PAT formation. Air-filled trachea, visualized by reflected light (white). Dashed circles, extent of PAT formation. Examples of PAT formation phenotypes are indicated, classified as in fig. S5E-H. **(C)** Frames from live imaging (see also Movie S2) at the indicated times APF of control and tracheal *bnl* RNAi knockdown pupae as in A. Progenitors (white, *btl-RFP-moe*) migrate along larval DT in control pupa, but they never leave the SB niche (dash) in the tracheal *bnl* knockdown pupa. Arrowheads, progenitor migration front; *, progenitor migration extends beyond field of view. **(D)** Frames from live imaging (see Movie S4) at the indicated times APF of a *dfr-FLP/ act5c>Y>Gal4, UAS-GFP; btl-RFP-moe/ UAS-bnl RNAi* pupa in which *bnl* expression was knocked down in a DT patch along the Tr5 DT (bracket). Tr4 progenitors are stalled next to the large patch, whereas Tr5 progenitors are not stalled by the smaller patches of *bnl* RNAi expression in the Tr6 DT. **(E)** Confocal fluorescent micrograph of a *UAS-FLP/ act5c>Y>Gal4, UAS-GFP; prd-Gal4, btl-RFP-moe/ UAS-bnl RNAi* pupa fixed following 6 hours of live-imaging (see Fig. 3D and Movie S3) and then stained for tracheal progenitors (anti-RFP, red), cells expressing *bnl RNAi* (anti-GFP, green), and nuclei (DAPI, blue). Optical sections at the planes indicated (s1 - s4) are shown. Progenitors stalled next to the short segment of DT, approximately 2 to 3 larval cells wide, in which *paired* FLP-out drives a patch of expression (bracket) of *UAS-bnl RNAi* and *UAS-GFP*. Optical sections show that *bnl RNAi* expressing cells encompass full circumference of DT. Bars, 50 µm (A and E), 100 µm (B-D).

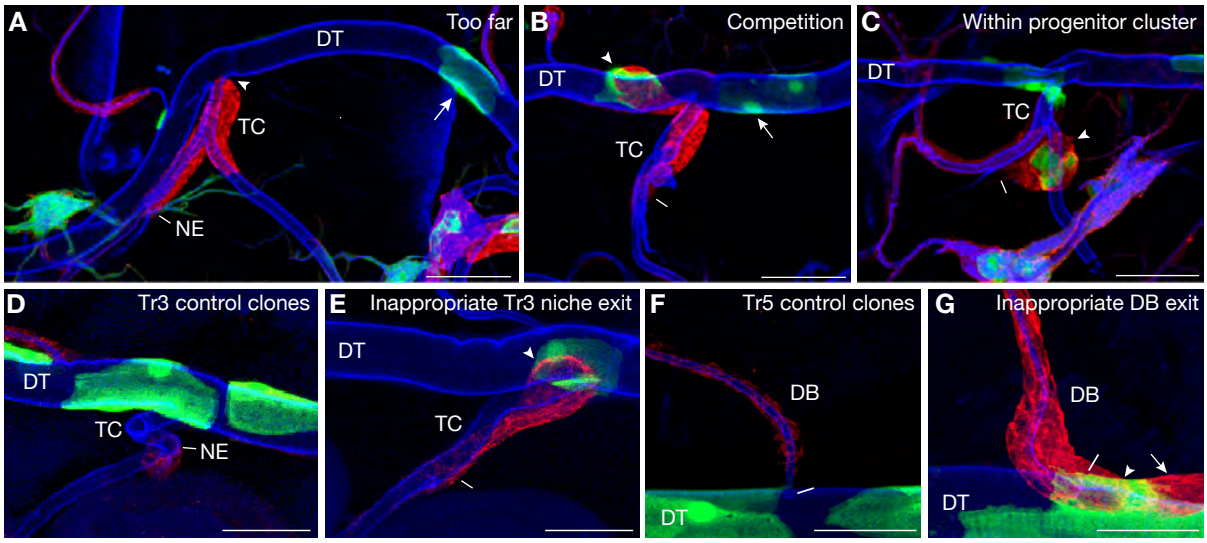

Figure S8. Examples of *branchless*-expressing clones that did not induce ectopic migration of PAT progenitors and clones that induced migration of progenitors that do not normally migrate. GFP-labeled clones of *bnl*-expressing cells (green) were induced and analyzed in wandering third-instar larvae as in Figure 4. Dash, niche exit (NE); DT, dorsal trunk; TC, transverse connective; DB, dorsal branch; arrowheads, progenitor migration front. **(A)** A clone (arrow) far from the Tr4 migrating progenitors (red) that did not induce ectopic progenitor migration. **(B)** A pair of clones (arrow and arrowhead) in which Tr5 progenitors have migrated toward only one of the clones (arrowhead). **(C)** A clone in the Tr5 progenitor cell cluster. Migration is disrupted and progenitors remain near the SB niche. **(D)** Control clones in Tr3. Tr3 progenitors normally remain within the SB niche during PAT outgrowth and are unaffected by control clones expressing only GFP. **(E)** A *bnl*-expressing clone that has recruited Tr3 progenitors out of the niche to DT. Note that the Tr3 progenitors have reached the DT clone even though there is no endogenous (or ectopic) *bnl* expression in the TC, perhaps because the Tr3 TC is shorter than those in other metameres. **(F)** Control clone near Tr5 DB. Progenitors in anterior DBs (Tr2 to Tr5) derived from de-differentiated larval cells express *btl-RFP-moe* (fig. S2A) and proliferate but normally remain in the DB niche (see also fig. S2A' and fig. S4B, C). **(G)** Tr5 DB progenitors (arrowhead) are sometimes recruited onto the DT by clones expressing ectopic *bnl*. Arrow, Tr5 SB progenitors also recruited by the clone. Dash, DB boundary at DB/DT junction. Bars, 100 µm (A-C), 50 µm (D-G).

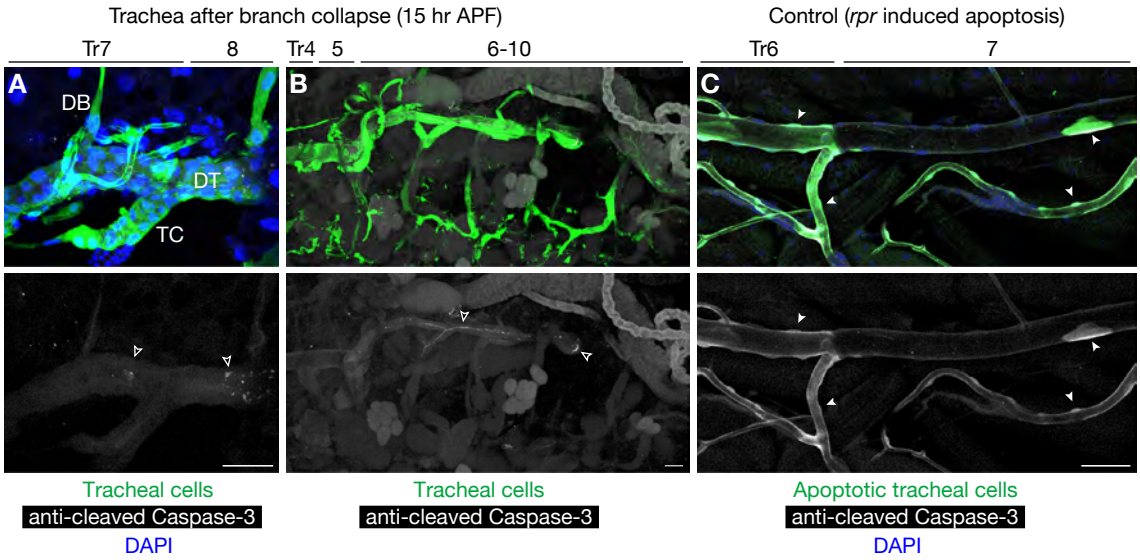

Figure S9. Decaying tracheal branches do not express cleaved Caspase-3. (A, B) Fluorescent micrographs of *ppk4>GFP; btl-RFP-moe* 15 hr APF pupae immunostained for cleaved Caspase-3 (white), a marker of apoptosis, and for GFP (green) to show tracheal cells. Nuclei are stained with DAPI (blue). Larval tracheal cells in posterior metameres (Tr6 to Tr10) are lost during metamorphosis *(10)* but are not stained by the cleaved Caspase-3 immunostain, suggesting that they die later in metamorphosis or by other mechanisms. Thin or spotty staining (open arrowheads) is antibody trapped in collapsed posterior tracheal branches (Fig. 1). **(C)** Fluorescent micrograph of a *ppk4-Gal4, UAS-GFP/ UAS-rpr; tub-Gal80ts/* + wandering third-instar larva stained as in A and B as a control to show cleaved Caspase-3 expression in apoptotic tracheal cells. Note cleaved Caspase-3 immunostaining (white) in tracheal cells activating expression of the apoptosis inducer *reaper* (*rpr*) and marked by GFP (green; arrowheads). Animals were raised at the permissive temperature (18° C) of the GAL80ts repressor to prevent early ectopic *rpr* expression and allow embryonic tracheal formation, and then transferred to the non-permissive temperature (30° C) to activate *rpr*-induced apoptosis. Bars, 50 µm.

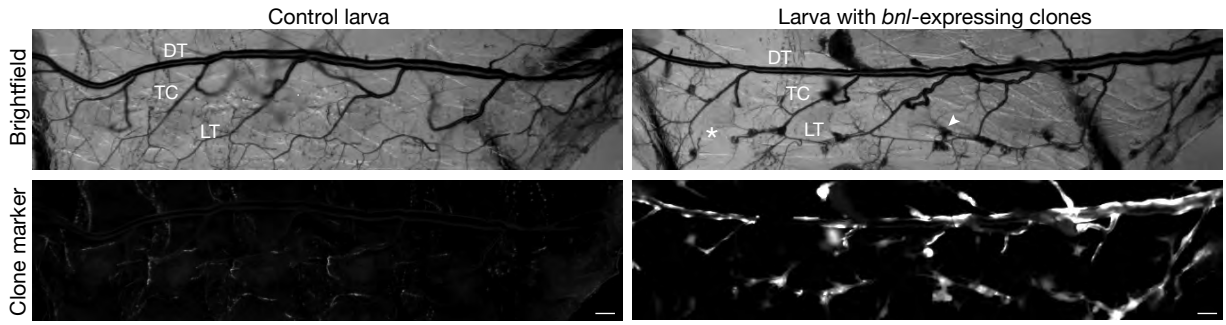

Figure S10. Effect on the larval tracheal system of tracheal clones expressing *branchless* FGF. Brightfield (upper) and fluorescence (lower) images of a control *Cyo/ act5c>Y>Gal4, UAS-GFP; btl-RFP-moe/ UAS-bnl* wandering third instar larva and a *dfr-FLP/ act5c>Y>Gal4, UAS-GFP; btl-RFP-moe/ UAS-bnl* larva in which the GFP-marked clones express ectopic *bnl*. Note tracheal patterning in the larva with *bnl*-expressing clones was not globally perturbed, although there are local defects including a sporadic gap (*) in the lateral trunk (LT) and scattered foci of densely-packed tracheoles (arrowhead). DT, dorsal trunk; TC, transverse connective. Bars, 100 µm.

1241442s1.mov

Movie S1. Tracheal progenitors migrating along the larval dorsal trunk. Fluorescence imaging of a live *btl-RFP-moe* white pupa beginning just after puparium formation (0 hr APF) in which migrating PAT progenitors originating from tracheal metameres Tr4 and Tr5 and expressing RFP-moesin (white; arrowheads) were visualized through the cuticle. Images were acquired every three minutes for seven hours at 25°C. DT, dorsal trunk; TC, transverse connective; dash, SB niche exit. Progenitors move toward the posterior at ~1.7 µm/min, maintaining a close association with the DT and crawling and wrapping around it as they migrate. Tr4 progenitors move onto DT about one hour later than Tr5 progenitors. Note multiple tips of migrating progenitors, each taking slightly different paths along DT into posterior. Bar, 100 µm.

1241442s2.mov

Movie S2. Effect of *branchless* knockdown on progenitors exiting SB niche. Fluorescence imaging of a live *ppk4-Gal4/ UAS-GFP; btl-RFP-moe/ UAS-bnl RNAi* pupa in which *bnl* was knocked down by RNAi in larval tracheal cells (marked by GFP, pseudo-colored green in merged images). Tracheal progenitors marked by RFP fluorescence and pseudo-colored red in merged images (arrowheads) do not move beyond niche exit (dash). DT, dorsal trunk; TC, transverse connective. Images were acquired every five minutes from 0 hr to 6 hr APF at 25°C. Bar, 100 µm.

1241442s3.mov

Movie S3. Effect of *branchless* knockdown in patch along Tr5 progenitor migration route. Live imaging of an *act5c>Y>Gal4, UAS-GFP/ UAS-FLP; prd-Gal4, btl-RFP-moe/ UAS-bnl RNAi* pupa in which *bnl* expression was inactivated in portion of Tr6 DT (bracket) by expression of *bnl RNAi* mediated by *paired-Gal4*. Tr5 tracheal progenitors move onto DT but stall when they reach DT patch where *bnl RNAi* is expressed; meanwhile, Tr4 progenitors progress posteriorly. DT, dorsal trunk; TC, transverse connective; dash, SB niche exit; arrowhead, progenitors. Images were acquired every five minutes from 0 hr to 6 hr APF at 25°C. Bar, 100 µm.

1241442s4.mov

Movie S4. Effect of *branchless* knockdown in patch along Tr4 progenitor migration route. Live imaging of a *dfr-flp / act5c>Y>Gal4, UAS-GFP; btl-RFP-moe/ UAS-bnl RNAi* pupa in which *bnl* expression was inactivated in a portion of Tr5 DT (bracket) by expression of *bnl RNAi*. Tr4 tracheal progenitors stall next to DT patch where *bnl RNAi* is expressed. DT, dorsal trunk; TC, transverse connective; dash, SB niche exit; arrowhead, progenitors. Images were acquired every five minutes from 0 hr to 6 hr APF at 25°C. Bar, 100 µm.

References and Notes

1. N. Barker, S. Bartfeld, H. Clevers, Tissue-resident adult stem cell populations of rapidly self-renewing organs. *Cell Stem Cell* **7**, 656–670 (2010). Medline doi:10.1016/j.stem.2010.11.016

2. G. B. Adams, D. T. Scadden, The hematopoietic stem cell in its place. *Nat. Immunol.* **7**, 333–337 (2006). Medline doi:10.1038/ni1331

3. A. Alvarez-Buylla, D. A. Lim, For the long run: Maintaining germinal niches in the adult brain. *Neuron* **41**, 683–686 (2004). Medline doi:10.1016/S0896-6273(04)00111-4

4. C. Blanpain, E. Fuchs, Epidermal homeostasis: A balancing act of stem cells in the skin. *Nat. Rev. Mol. Cell Biol.* **10**, 207–217 (2009). Medline doi:10.1038/nrm2636

5. E. Sancho, E. Batlle, H. Clevers, Live and let die in the intestinal epithelium. *Curr. Opin. Cell Biol.* **15**, 763–770 (2003). Medline doi:10.1016/j.ceb.2003.10.012

6. G. L. Ming, H. Song, Adult neurogenesis in the mammalian brain: Significant answers and significant questions. *Neuron* **70**, 687–702 (2011). Medline doi:10.1016/j.neuron.2011.05.001

7. E. Nacu, E. M. Tanaka, Limb regeneration: A new development? *Annu. Rev. Cell Dev. Biol.* **27**, 409–440 (2011). Medline doi:10.1146/annurev-cellbio-092910-154115

8. K. D. Poss, Advances in understanding tissue regenerative capacity and mechanisms in animals. *Nat. Rev. Genet.* **11**, 710–722 (2010). Medline doi:10.1038/nrg2879

9. T. Matsuno, Morphogenesis of pupal abdominal tracheae in a fruit fly, *Drosophila melanogaster*. *Jap. J. Appl. Entomol. Zool.* **34**, 165–167 (1990). doi:10.1303/jjaez.34.165

10. G. Manning, M. A. Krasnow, in *The Development of* Drosophila melanogaster, M. Bate, A. Martinez-Arias, Eds. (Cold Spring Harbor Laboratory Press, Woodbury, NY, 1993), vol. 1, pp. 609–685.

11. M. Weaver, M. A. Krasnow, Dual origin of tissue-specific progenitor cells in *Drosophila* tracheal remodeling. *Science* **321**, 1496–1499 (2008). doi:10.1126/science.1158712

12. A. Guha, L. Lin, T. B. Kornberg, Organ renewal and cell divisions by differentiated cells in *Drosophila*. *Proc. Natl. Acad. Sci. U.S.A.* **105**, 10832–10836 (2008). Medline doi:10.1073/pnas.0805111105

13. C. Pitsouli, N. Perrimon, Embryonic multipotent progenitors remodel the *Drosophila* airways during metamorphosis. *Development* **137**, 3615–3624 (2010). Medline doi:10.1242/dev.056408

14. M. Sato, Y. Kitada, T. Tabata, Larval cells become imaginal cells under the control of homothorax prior to metamorphosis in the *Drosophila* tracheal system. *Dev. Biol.* **318**, 247–257 (2008). Medline doi:10.1016/j.ydbio.2008.03.025

15. C. Ribeiro, M. Neumann, M. Affolter, Genetic control of cell intercalation during tracheal morphogenesis in *Drosophila*. *Curr. Biol.* **14**, 2197–2207 (2004). Medline doi:10.1016/j.cub.2004.11.056

16. L. Liu, W. A. Johnson, M. J. Welsh, *Drosophila* DEG/ENaC pickpocket genes are expressed in the tracheal system, where they may be involved in liquid clearance. *Proc. Natl. Acad. Sci. U.S.A.* **100**, 2128–2133 (2003). Medline doi:10.1073/pnas.252785099

17. K. Guillemin, J. Groppe, K. Ducker, R. Treisman, E. Hafen, M. Affolter, M. A. Krasnow, The *pruned* gene encodes the *Drosophila* serum response factor and regulates cytoplasmic outgrowth during terminal branching of the tracheal system. *Development* **122**, 1353–1362 (1996). Medline

18. C. Klämbt, L. Glazer, B. Z. Shilo, Breathless, a *Drosophila* FGF receptor homolog, is essential for migration of tracheal and specific midline glial cells. *Genes Dev.* **6**, 1668–1678 (1992). Medline doi:10.1101/gad.6.9.1668

19. M. Reichman-Fried, B. Z. Shilo, Breathless, a *Drosophila* FGF receptor homolog, is required for the onset of tracheal cell migration and tracheole formation. *Mech. Dev.* **52**, 265–273 (1995). Medline doi:10.1016/0925-4773(95)00407-R

20. D. Sutherland, C. Samakovlis, M. A. Krasnow, *branchless* encodes a *Drosophila* FGF homolog that controls tracheal cell migration and the pattern of branching. *Cell* **87**, 1091–1101 (1996). Medline doi:10.1016/S0092-8674(00)81803-6

21. J. Jarecki, E. Johnson, M. A. Krasnow, Oxygen regulation of airway branching in *Drosophila* is mediated by *branchless* FGF. *Cell* **99**, 211–220 (1999). Medline doi:10.1016/S0092-8674(00)81652-9

22. M. Sato, T. B. Kornberg, FGF is an essential mitogen and chemoattractant for the air sacs of the *Drosophila* tracheal system. *Dev. Cell* **3**, 195–207 (2002). Medline doi:10.1016/S1534-5807(02)00202-2

23. Materials and methods are available as supporting material on *Science* Online.

24. S. Hayashi, K. Ito, Y. Sado, M. Taniguchi, A. Akimoto, H. Takeuchi, T. Aigaki, F. Matsuzaki, H. Nakagoshi, T. Tanimura, R. Ueda, T. Uemura, M. Yoshihara, S. Goto, GETDB, a database compiling expression patterns and molecular locations of a collection of Gal4 enhancer traps. *Genesis* **34**, 58–61 (2002). Medline doi:10.1002/gene.10137

25. M. Buszczak, S. Paterno, D. Lighthouse, J. Bachman, J. Planck, S. Owen, A. D. Skora, T. G. Nystul, B. Ohlstein, A. Allen, J. E. Wilhelm, T. D. Murphy, R. W. Levis, E. Matunis, N. Srivali, R. A. Hoskins, A. C. Spradling, The Carnegie protein trap library: A versatile tool for *Drosophila* developmental studies. *Genetics* **175**, 1505–1531 (2007). Medline doi:10.1534/genetics.106.065961

26. A. H. Brand, N. Perrimon, Targeted gene expression as a means of altering cell fates and generating dominant phenotypes. *Development* **118**, 401–415 (1993). Medline

27. P. Steneberg, C. Englund, J. Kronhamn, T. A. Weaver, C. Samakovlis, Translational readthrough in the *hdc* mRNA generates a novel branching inhibitor in the *Drosophila* trachea. *Genes Dev.* **12**, 956–967 (1998). Medline doi:10.1101/gad.12.7.956

28. G. J. Beitel, M. A. Krasnow, Genetic control of epithelial tube size in the *Drosophila* tracheal system. *Development* **127**, 3271–3282 (2000). Medline

29. S. J. Marygold, P. C. Leyland, R. L. Seal, J. L. Goodman, J. Thurmond, V. B. Strelets, R. J. Wilson; FlyBase consortium, FlyBase: Improvements to the bibliography. *Nucleic Acids Res.* **41**, D751–D757 (2013). Medline doi:10.1093/nar/gks1024

30. G. Dietzl, D. Chen, F. Schnorrer, K. C. Su, Y. Barinova, M. Fellner, B. Gasser, K. Kinsey, S. Oppel, S. Scheiblauer, A. Couto, V. Marra, K. Keleman, B. J. Dickson, A genome-wide transgenic RNAi library for conditional gene inactivation in *Drosophila*. *Nature* **448**, 151–156 (2007). Medline doi:10.1038/nature05954

31. D. Sutherland, thesis, Stanford University (1999).

32. K. G. Golic, S. Lindquist, The FLP recombinase of yeast catalyzes site-specific recombination in the *Drosophila* genome. *Cell* **59**, 499–509 (1989). Medline doi:10.1016/0092-8674(89)90033-0

33. K. Certel, M. G. Anderson, R. J. Shrigley, W. A. Johnson, Distinct variant DNA-binding sites determine cell-specific autoregulated expression of the *Drosophila* POU domain transcription factor *drifter* in midline glia or trachea. *Mol. Cell. Biol.* **16**, 1813–1823 (1996). Medline

34. K. Ito, W. Awano, K. Suzuki, Y. Hiromi, D. Yamamoto, The *Drosophila* mushroom body is a quadruple structure of clonal units each of which contains a virtually identical set of neurones and glial cells. *Development* **124**, 761–771 (1997). Medline

35. J. Huang, W. Zhou, W. Dong, A. M. Watson, Y. Hong, Directed, efficient, and versatile modifications of the *Drosophila* genome by genomic engineering. *Proc. Natl. Acad. Sci. U.S.A.* **106**, 8284–8289 (2009). Medline doi:10.1073/pnas.0900641106

36. M. G. Anderson, G. L. Perkins, P. Chittick, R. J. Shrigley, W. A. Johnson, *drifter*, a *Drosophila* POU-domain transcription factor, is required for correct differentiation and migration of tracheal cells and midline glia. *Genes Dev.* **9**, 123–137 (1995). Medline doi:10.1101/gad.9.1.123

37. M. Ashburner, K. G. Golic, R. S. Hawley, *Drosophila: A Laboratory Handbook* (Cold Spring Harbor Laboratory Press, Cold Spring Harbor, NY, ed. 2, 2005).

38. B. P. Levi, A. S. Ghabrial, M. A. Krasnow, *Drosophila* talin and integrin genes are required for maintenance of tracheal terminal branches and luminal organization. *Development* **133**, 2383–2393 (2006). Medline doi:10.1242/dev.02404

39. N. Hacohen, S. Kramer, D. Sutherland, Y. Hiromi, M. A. Krasnow, *sprouty* encodes a novel antagonist of FGF signaling that patterns apical branching of the *Drosophila* airways. *Cell* **92**, 253–263 (1998). Medline doi:10.1016/S0092-8674(00)80919-8